An Assembly Route to Inorganic Catalytic Nanoreactors Containing Sub-10-nm Gold Nanoparticles with Anti-Aggregation Properties**

Xiaoqing Huang, Changyou Guo, Jinquan Zuo, Nanfeng Zheng, and Galen D. Stucky**

Noble metal nanoparticles are attractive as catalysts due to their large surface area-to-volume ratios.[1–4] Appropriately sized noble metal nanoparticles such as supported gold nanoparticles can exhibit unique catalytic properties that are not revealed in their bulk forms.[5–11] Having highly active surface atoms, however, often leads to changes in the size and shape of nanoparticles during catalysis and therefore a rapid decay in their catalytic abilities.[12–14] The challenge of preparing highly active nanocatalysts based on sub-10 nm metal nanoparticles that have an acceptable long-term stability remains to be solved.

In order to suppress the sintering of metal nanoparticles during catalysis or high-temperature thermal treatment, two strategies are widely employed: i) depositing nanoparticles on high-surface area substances, and ii) confining them in the channels or void spaces of porous materials.[1,15–18] In both of these two approaches, however, the slow sintering of nanoparticles is inevitable. From a structural point of view, core–shell materials with metal nanoparticle cores are desirable to preventing nanoparticles from sintering, and have therefore recently received much attention for catalysis applications.[19–23] To achieve high catalysis performance, the metal nanoparticle core should be highly accessible by reactants, whilst the shell should allow the fast diffusion of both reactants and products. Encapsulating nanoparticles in hollow porous spheres as yolk–shell nanoreactors represents an effective method to create such core–shell materials for catalysis.[24,25]

Compared to conventional catalysts embedded in bulk supports, each nanoparticle in the yolk–shell nanoreactor is isolated by a highly porous shell and has a relatively homogeneous surrounding environment. The interaction and sintering between core metal nanoparticles can be effectively hindered, even under harsh conditions, by making the pore size in the shell smaller than the size of the core nanoparticles. Yolk–shell structured nanoreactors for catalysis have typically been fabricated by multistep assembly pathways starting from pre-synthesized metal nanoparticles. Currently, the synthesis of yolk–shell nanoreactors is dominated by use of hydrophilic particles as the precursor.[23–25] In the case of gold, only reactors with core nanoparticle sizes larger than 10 nm have been explored. Song et al. have recently used KCN to selectively etch the core Au in $Au@SiO_2$ and therefore control the size of Au nanoparticles in the range of tens of nanometers.[23] However, the challenge of encapsulating gold nanoparticles at <10 nm in yolk–shell nanoreactors remains. No attempt has yet been made to utilize sub-10 nm thiol-capped gold nanoparticles, a class of widely studied nanoparticles, for the fabrication of yolk–shell catalytic nanoreactors.[26]

We report here an assembly route to prepare yolk–shell catalytic nanoreactors with a core of a 6.3 nm Au nanoparticle and a mesoporous ZrO_2 or TiO_2 shell, starting from monodisperse hydrophobic Au nanoparticles. The overall size of the nanoreactors is ~150 nm. The resulting nanoreactors exhibit remarkable catalytic activity in the reduction of 4-nitrophenol by $NaBH_4$. The yolk–shell structure design of the nanoreactors endows the Au nanoparticles trapped inside with excellent anti-aggregation properties upon thermal treatment.

Scheme 1 illustrates the procedure for creating Au@hollow mesoporous-ZrO_2 (Au@*hm*-ZrO_2) nanoreactors. To make catalytic nanoreactors having sub-10 nm Au nanoparticle cores, we chose dodecanethiol-capped 6.3 nm Au nanoparticles as the starting material for the catalytic core. Monodisperse thiol-capped Au nanoparticles are first prepared and ligand-exchanged with mercaptoundecanoic acid to make them water soluble in the presence of NH_3.[27,28] Through the modified Stöber method, the water-soluble Au particles are then coated with a silica layer to obtain the core–shell $Au@SiO_2$ composite.

As shown in Figure 1a, $Au@SiO_2$ spheres having a uniform diameter of about 120 nm and containing only one Au nanoparticle at the center of each sphere have been successfully prepared through careful control over hydrolysis

[*] Prof. N. Zheng, X. Huang, Dr. C. Guo, J. Zuo
State Key Laboratory for Physical Chemistry of Solid Surfaces and Department of Chemistry
Xiamen University, Xiamen 361005 (P. R. China)
E-mail: nfzheng@xmu.edu.cn
Prof. G. D. Stucky
Department of Chemistry and Biochemistry
University of California, Santa Barbara, CA 93106 (USA)
E-mail: stucky@chem.ucsb.edu

[**] We thank the Chinese Ministry of Education (Key Project 108077), NNSFC (20871100, 20721001, 20423002), the 973 projects (2007CB815303, 2009CB930703) from MSTC, and NFFTBS (No. J0630429) for support of this work.

DOI: 10.1002/smll.200800808

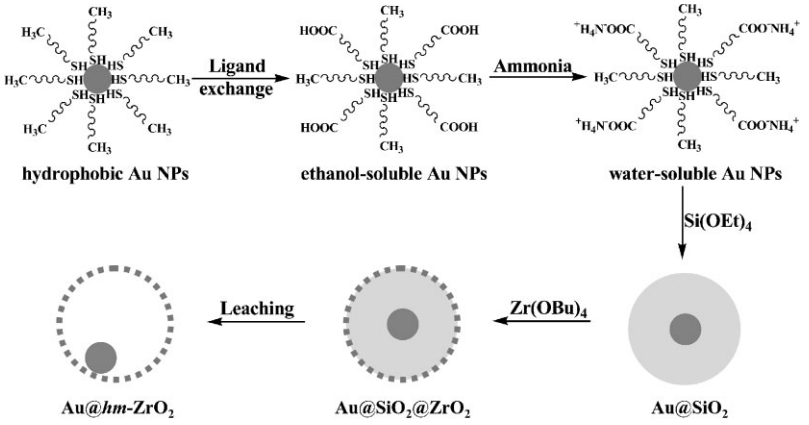

Scheme 1. Synthetic procedure of Au@*hm*-ZrO_2 nanoreactors.

conditions. The uniform Au@SiO_2 spheres are then coated with a layer of zirconia through the hydrolysis of $Zr(OBu)_4$ in the presence of Brij 30 surfactant using a modified literature method.[24,29] After being aged in water for 12 h, the particles are calcined at 850 °C. Treatment with NaOH solution (5 M) is then applied to remove the silica layer in the calcined Au@SiO_2@ZrO_2 (Figure 1b) to create Au@*hm*-ZrO_2 nanoreactors (Figure 1c). The thickness of the porous ZrO_2 layer is approximately 15 nm. With the creation of the hollow space, the Au nanoparticles are deposited somewhere inside the hollow zirconia sphere, no longer at the center. The energy dispersive X-ray spectrum (EDX) of the nanoreactors shows that a small amount of silica remains in the porous shell. The X-ray diffraction data (XRD) demonstrates the amorphous nature of silica and the tetragonal nanocrystalline feature of zirconia in both calcined Au@SiO_2@ZrO_2 and Au@*hm*-ZrO_2 nanoreactors. We have also successfully applied a similar preparation procedure to create Au@*hm*-TiO_2 nanoreactors with a TiO_2 thickness of about 20 nm (Figure 1d and e). Meanwhile, the size of core particles can be varied when thiol-capped Au nanoparticles with different sizes are used as the precursors. For example, we also obtained nanoreactors with 3.5 nm Au nanoparticles as the core (see Supporting Information, Figure S6).

At the first level, to be an efficient catalyst, the shell of yolk–shell nanoreactors should be so permeable to both reactants and products that mass-transfer limitations can be avoided to maximize the reaction rates. High porosity of the zirconia shell in the prepared nanoreactors is then crucial for their catalysis applications. N_2 adsorption measurements do confirm the highly porous nature of the zirconia shell in the prepared Au@*hm*-ZrO_2 nanoreactors. A typical N_2 adsorption/desorption isotherm for Au@*hm*-ZrO_2 samples is shown in Figure 2. The Brunauer–Emmett–Teller (BET) surface area and pore volume of the as-synthesized nanoreactors are $222\,m^2 \cdot g^{-1}$ and $0.233\,cm^3 \cdot g^{-1}$, respectively. The inset of Figure 2 shows the pore size distribution of the Au@*hm*-ZrO_2 nanoreactors obtained from the analysis of the adsorption branch of the isotherm using the Barrett–Joyner–Halenda (BJH) method. The as-made Au@*hm*-ZrO_2 has a rather narrow size distribution centered at 1.6 nm, which is smaller than the size of the Au nanoparticles inside the nanoreactors.

We performed the catalytic reduction of 4-nitrophenol by $NaBH_4$, which does not progress at room temperature without the use of catalyst,[23,30] in order to evaluate the accessibility and catalytic performance of Au nanoparticles in the prepared nanoreactors. In the presence of Au@*hm*-ZrO_2, the reaction goes to completion with the production of 4-aminophenol (Figure 3). The reduction kinetics were monitored by UV-vis absorption spectroscopy of the reaction mixture after addition of Au@*hm*-ZrO_2. According to the time-domain spectra, the absorption of 4-nitrophenol at 400 nm decreases with a concomitant increase of the 295 nm peak of 4-aminophenol within 12 min after the catalyst introduction (Figure 3a). The presence of an isosbestic point at 313 nm indicates that only 4-aminophenol is produced from the catalytic reduction of 4-nitrophenol. Therefore, the conversion process can be read directly from the time-domain spectra as the ratio of 4-nitrophenol concentration at time t and 0 (C_t/C_0) corresponds to the ratio of the respective absorbance (A_t/A_0) at 400 nm. Considering that the concentration of $NaBH_4$ largely exceeds that of 4-nitrophenol, the reduction rate is assumed to

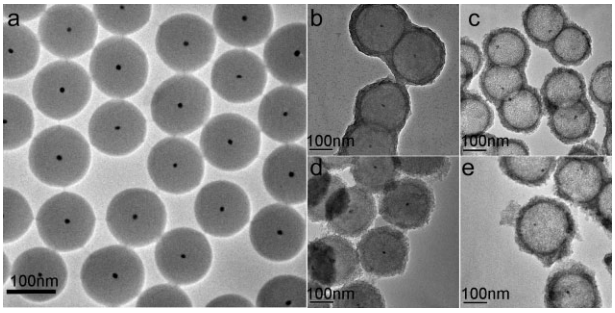

Figure 1. TEM images of a) Au@SiO_2, b) Au@SiO_2@ZrO_2, c) Au@*hm*-ZrO_2, d) Au@SiO_2@TiO_2, and e) Au@*hm*-TiO_2.

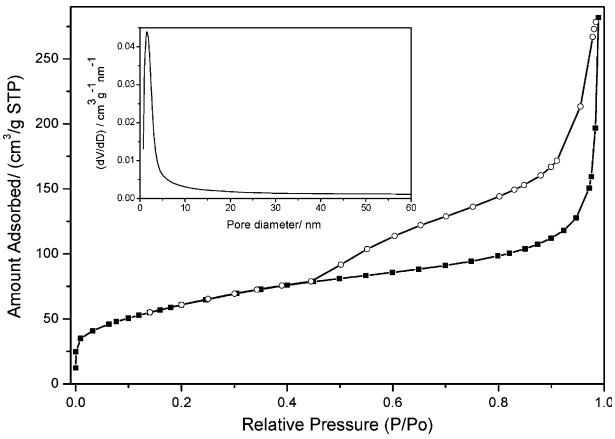

Figure 2. Nitrogen adsorption/desorption isotherms and pore-size distribution (inset) of Au@*hm*-ZrO_2 nanoreactors.

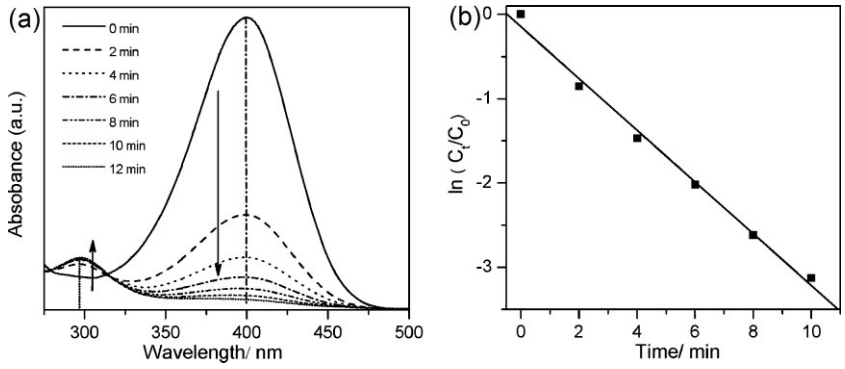

Figure 3. a) The time-domain UV-vis spectra of the reaction mixture and b) the linear relationship between $\ln(C_t/C_0)$ and reaction time during the course of reduction of 4-nitrophenol catalyzed by Au@*hm*-ZrO_2. The arrows indicate the increase of reaction time.

be independent of the $NaBH_4$ concentration. A linear relation between $\ln(C_t/C_0)$ and reaction time is observed (Figure 3b). The experimental results show that the catalytic reduction of 4-nitrophenol follows pseudo first-order rate kinetics with respect to 4-nitrophenol concentration. The rate constant of the reaction for the reduction of 4-nitrophenol by the Au@*hm*-ZrO_2 nanocatalyst is calculated to be 0.31 min^{-1}.

With size larger than the pore size within the reactor shell, the Au nanoparticles in the prepared nanoreactors are expected to have anti-aggregation properties during catalysis or under high-temperature thermal treatment. To establish this, as-prepared Au@*hm*-ZrO_2 nanoreactors were subjected to thermal treatment in air for 2 h at 300 °C, at 550 °C, and at 750 °C. When the thermally treated samples were used as catalysts for the reduction of 4-nitrophenol, they exhibited catalytic activity similar to the original untreated sample (Figure 4a), which indicates that Au nanoparticles in Au@*hm*-ZrO_2 nanoreactors are highly stable against thermal sintering. To demonstrate the advantages of the yolk–shell structure in stabilizing metal nanoparticles over surface-supported structures, we prepared catalysts with 6.3 nm Au nanoparticles deposited on the surface rather inside the hollow mesoporous ZrO_2 spheres. As shown in Figure 4a, the catalytic activity of surface-supported Au nanoparticles decreases dramatically with the thermal treatment temperature, which elucidates that the yolk–shell configuration is indeed a superior architecture for designing nanoparticle-based catalysts.

We also investigated the reusability of the Au@*hm*-ZrO_2 catalyst to study the anti-aggregation properties of Au nanoparticles during catalysis. The yolk–shell nanoreactors were separated from the reaction mixture by centrifugation and redispersed into a fresh solution through mild ultrasonication. The recycled catalysts exhibit similar catalytic activity to the original nanoreactors (Figure 4b). There is only a slight decrease in the activity between the reused and fresh catalyst. Such a small decrease of catalytic activity is probably due to incomplete separation of the catalyst from the reaction solution. In contrast, an obvious decrease in catalytic activity is seen for reused surface-supported Au nanoparticles (Figure 4b) in which Au nanoparticles are deposited on the surface of hollow mesoporous ZrO_2.

In order to demonstrate the synergetic effect between the Au nanoparticle core and the porous oxide shell, we also tested the catalytic activity of nanoreactors with different shell compositions toward CO oxidation. The reactions were carried out on nanoreactors with Au nanoparticles of the same size (6.3 nm) as the core but with different shell materials (i.e., TiO_2, ZrO_2). As shown in Figure 5, no significant activity is observed for Au@*hm*-ZrO_2 nanoreactors. Although an

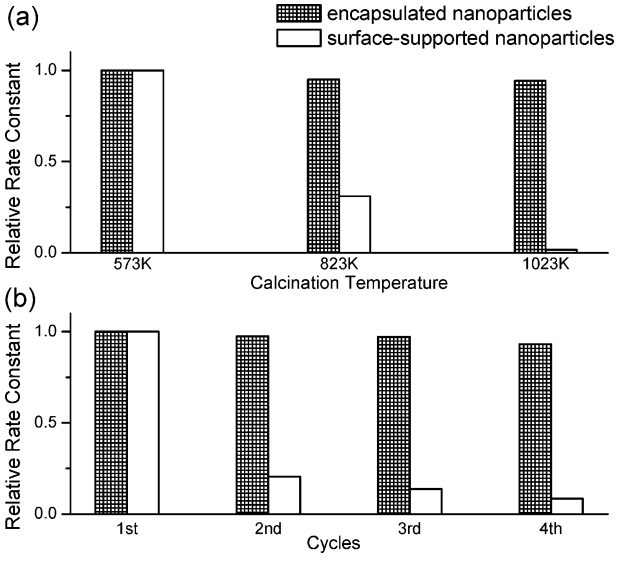

Figure 4. a) The effect of thermal treatment temperature on the catalysis activity of Au nanoparticles encapsulated and supported on the hollow mesoporous ZrO_2 spheres. b) A comparison of catalysis activity for both encapsulated and surface-supported Au nanoparticles on hollow mesoporous ZrO_2 during the four cycles of use.

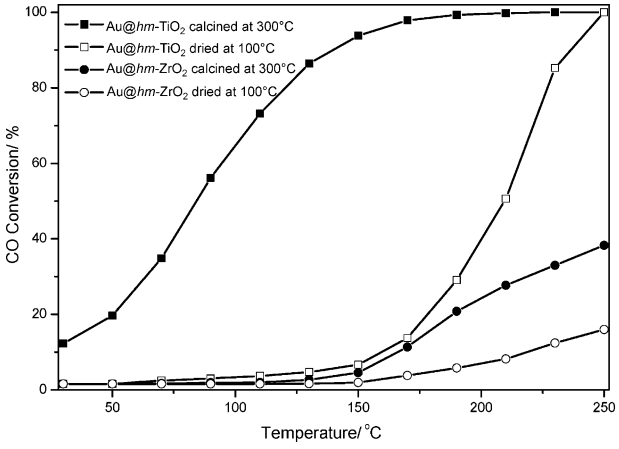

Figure 5. A comparison of catalysis activity in CO oxidation by Au@*hm*-TiO_2 and Au@*hm*-ZrO_2 nanoreactors treated at 100 °C and 300 °C. Catalytic conditions: 50 mg catalyst, 50 mL 1% CO balanced with air.

improvement can be achieved by thermal treatment (i.e., 2 h at 300 °C) or pre-treatment under H_2 atmosphere (Figure S7), the catalytic activity of Au@*hm*-ZrO_2 nanoreactors is still quite limited. In comparison, nanoreactors with TiO_2 shells display much better performance, particularly after being calcined at 300 °C (Figure 5). This result suggests that the shell materials could be a crucial factor in the design of efficient encapsulated-type catalysts. It should be noted that the Au loading in both Au@*hm*-TiO_2 and Au@*hm*-ZrO_2 used for the catalysis is less than 0.3 wt%. With such a low Au loading, the activity of Au@*hm*-TiO_2 nanoreactors in CO oxidation is significant. Furthermore, with Au nanoparticles encapsulated in the nanoreactors, we did not observe any activity decay with time in a 48 h experiment.

In conclusion, monodisperse hydrophobic Au nanoparticles have been successfully used as the base materials for the fabrication of yolk–shell catalytic nanoreactors through an assembly approach. Owing to the structural feature that only one Au nanoparticle is encapsulated in each hollow sphere, which is highly porous but with a pore size smaller than the size of the Au nanoparticle, the nanoreactors demonstrate both a remarkable catalytic activity and anti-aggregation properties during the course of catalysis or upon thermal treatment. Although the large-scale synthesis of monodisperse hydrophobic metal nanoparticles with different compositions and sizes has been widely achieved in the past decade, their direct applications in catalysis have been rarely reported due to their catalytic inertness. The synthetic route reported here serves as an excellent example of demonstrating the feasibility of converting these catalytically inert particles into highly efficient and stable nanocatalysts.

Experimental Section

Gold Nanoparticles: DDodecanethiol-capped Au nanoparticles were prepared according to the literature.[27] $AuPPh_3Cl$ (5 mmol) was mixed with dodecanethiol (2.5 mL) in benzene (400 mL) to form a clear solution to which *tert*-butylamine-borane (50 mmol) complex powders were then added in one portion. The mixture was heated with stirring at 55 °C for 1 h before the mixture was cooled to room temperature. Ethanol (400 mL) was then added to the reaction mixture to precipitate out Au nanoparticles as black solid powders. The solid product was separated by centrifugation, washed with excess ethanol, and dried under vacuum. Then, the solid product obtained above (0.1 g) was mixed with mercaptoundecanoic acid (0.1 g) in ethanol (10 mL) and ultrasonicated for 2 h. Concentrated ammonia (0.5 mL) was added to precipitate out the Au nanoparticles. The solid products were separated by centrifugation, washed with ethanol twice, and redispersed in water (4 mL) for further use.

Au@SiO_2 Core–Shell Particles: Aqueous Au colloidal solution (0.05 mL), concentrated ammonia (1.5 mL), and water (10 mL) were added to ethanol (50 mL). After stirring for 30 min, tetraethoxysilane (TEOS) (1 mL) was added. The reaction mixture was further stirred for 8 h. The resultant colloids were centrifuged and washed twice with water and twice with absolute ethanol. The solid was then redispersed in absolute ethanol (40 mL) for further use.

Au@SiO_2@ZrO_2 Core–Shell Particles: Au@SiO_2 core–shell colloids (6 mL), water (0.1 mL), and Birj 30 (0.1 mL) were added to ethanol (40 mL). After stiring for 30 min, $Zr(OBu)_4$ (0.2 mL) was added. The reaction mixture was stirred for another 8 h. The products were collected through centrifugation, redispersed in water (40 mL), and aged for 12 h. Removal of the organics and crystallization of zirconia were achieved by heating the particles in air from room temperature to 850 °C at the rate of 2.5 °C min^{-1} and kept at 850 °C for 2 h before cooling to room temperature.

Au@hm-ZrO_2 Yolk–Shell Particles: Silica was removed from the Au@SiO_2@ZrO_2 composites by treatment with NaOH (5 M) for 20 h. Finally, the particles were washed with ethanol and water. After silica removal, parts of the sample were also subjected to thermal treatment in air at 300, 550, and 750 °C for 2 h, respectively for thermal stability studies.

Gold Nanoparticles Supported on the Surface of hm-ZrO_2: The surface-supported Au nanoparticle catalysts were prepared following the protocol that we have recently developed.[28] Dodecanethiol-capped Au nanoparticles (10 mg) were first dispersed in chloroform (8 mL) to form a homogeneous solution to which pre-made *hm*-ZrO_2 (200 mg) were added in one portion. The mixture was stirred at room temperature for 2 h before the solid was separated by centrifugation, washed with chloroform, and dried at 100 °C. The sample was then calcined at 300 °C in air for 2 h to remove the organic capping agents. The calcined sample was then divided into three parts. Two parts of the sample were also further thermally treated in air for 2 h at 550 and 750 °C respectively to examine the stability upon thermal treatment.

Catalytic Reduction of p-Nitrophenol: An Au@*hm*-ZrO_2 nanoreactor suspension in water (0.40 mL, 6.25×10^{-5} M with respect to the gold precursor concentration) was added to $NaBH_4$ aqueous solution (1 mL, 1.2 M), and the mixture was stirred for 10 min at room temperature. 4-Nitrophenol (1 mL, 6.8×10^{-3} M) was then added to the mixture, which was stirred until the deep yellow solution became colorless. During the course of reaction, the reaction progress was monitored by measuring UV-vis absorption spectra of the mixture.

Keywords:
anti-aggregation · catalysts · encapsulation · gold · nanoparticles

[1] D. Astruc, F. Lu, J. R. Aranzaes, *Angew. Chem. Int. Ed.* **2005**, *44*, 7852.
[2] G. A. Somorjai, A. M. Contreras, M. Montano, R. M. Rioux, *Proc. Natl. Acad. Sci. USA* **2006**, *103*, 10577.
[3] N. Toshima, in *Nanoscale Materials* (Eds: L. M. Liz-Marzán, P. V. Kamat), Kluwer Academic Publishers, Boston **2003**, pp. 79–96.
[4] Q. Wang, A. E. Ostafin, in *Encyclopedia of Nanoscience and Nanotechnology*, Vol. 5(Ed: H. S. Nalwa), American Scientific Publishers, Stevenson Ranch, CA **2004**, pp. 475–503.
[5] G. C. Bond, D. T. Thompson, *Catal. Rev. - Sci. Eng.* **1999**, *41*, 319.
[6] T. V. Choudhary, D. W. Goodman, *Top. Catal.* **2002**, *21*, 25.
[7] T. V. Choudhary, D. W. Goodman, *Appl. Catal. A* **2005**, *291*, 32.
[8] M. Haruta, *Catal. Today* **1997**, *36*, 153.
[9] M. Haruta, *Cattech* **2002**, *6*, 102.
[10] M. Haruta, *Gold Bull.* **2004**, *37*, 27.
[11] G. J. Hutchings, *Catal. Today* **2005**, *100*, 55.
[12] R. Narayanan, M. A. El-Sayed, *J. Am. Chem. Soc.* **2004**, *126*, 7194.
[13] A. Roucoux, J. Schulz, H. Patin, *Chem. Rev.* **2002**, *102*, 3757.
[14] S. N. Sidorov, I. V. Volkov, V. A. Davankov, M. P. Tsyurupa, P. M. Valetsky, L. M. Bronstein, R. Karlinsey, J. W. Zwanziger, V. G.

Matveeva, E. M. Sulman, N. V. Lakina, E. A. Wilder, R. J. Spontak, *J. Am. Chem. Soc.* **2001**, *123*, 10502.
[15] E. G. Derouane, *Microporous and Mesoporous Solid Catalysts*, Wiley, Chichester, UK 2006.
[16] G. A. Somorjai, R. M. Rioux, *Catal. Today* **2005**, *100*, 201.
[17] J. M. Thomas, R. Raja, *Stud. Surf. Sci. Catal.* **2004**, *148*, 163.
[18] G. Ertl, H. Knözinger, J. Weitkamp, *Handbook of Heterogeneous Catalysis*, Wiley-VCH, Weinheim 1997.
[19] Y. D. Yin, R. M. Rioux, C. K. Erdonmez, S. Hughes, G. A. Somorjai, A. P. Alivisatos, *Science* **2004**, *304*, 711.
[20] M. Casavola, R. Buonsanti, G. Caputo, P. D. Cozzoli, *Eur. J. Inorg. Chem.* **2008**, 837.
[21] J. Bao, J. He, Y. Zhang, Y. Yoneyama, N. Tsubaki, *Angew. Chem. Int. Ed.* **2008**, *47*, 353.
[22] S. Takenaka, H. Umebayashi, E. Tanabe, H. Matsune, M. Kishida, *J. Catal.* **2007**, *245*, 392.
[23] J. Lee, J. C. Park, H. Song, *Adv. Mater.* **2008**, *20*, 1523.
[24] P. M. Arnal, M. Comotti, F. Schüth, *Angew. Chem. Int. Ed.* **2006**, *45*, 8224.
[25] S. Ikeda, S. Ishino, T. Harada, N. Okamoto, T. Sakata, H. Mori, S. Kuwabata, T. Torimoto, M. Matsumura, *Angew. Chem. Int. Ed.* **2006**, *45*, 7063.
[26] M. C. Daniel, D. Astruc, *Chem. Rev.* **2004**, *104*, 293.
[27] N. Zheng, J. Fan, G. D. Stucky, *J. Am. Chem. Soc.* **2006**, *128*, 6550.
[28] N. Zheng, G. D. Stucky, *J. Am. Chem. Soc.* **2006**, *128*, 14278.
[29] P. M. Arnal, C. Weidenthaler, F. Schüth, *Chem. Mater.* **2006**, *18*, 2733.
[30] K. Hayakawa, T. Yoshimura, K. Esumi, *Langmuir* **2003**, *19*, 5517.

Received: June 8, 2008
Revised: September 15, 2008
Published online: January 15, 2009

